

1

Optimization-Based Computational 2 Models of Retinal Cone Photoreceptor 3 Mosaic Formation

4 by

5 **James Magraken**

6 Thesis Submitted in Partial Fulfillment of the
7 Requirements for the Degree of
8 Computer Science and Mathematics BSc. Honours

9 in the
10 Department of Mathematics and Statistics
11 Faculty of Science

12 © James Magraken 2025
13 SIMON FRASER UNIVERSITY
14 June 2025

15 Copyright in this work is held by the author. Please ensure that any reproduction
or re-use is done in accordance with the relevant national copyright legislation.

¹⁶ Abstract

¹⁷ Many tissues in the central nervous system have cells organized in repetitive patterns that
¹⁸ are crucial to their function. In the vertebrate retina, cone photoreceptors often exhibit
¹⁹ precise patterning, with the highest regularities found in the lattice-like mosaics of fishes
²⁰ and geckos. Marine fishes in particular undergo a transformation from a hexagonal mosaic
²¹ of single cones, where each cone is surrounded by six neighbours, as present in the human
²² fovea, to a square mosaic, where each single cone is flanked by four double cones (i.e., two
²³ cones structurally linked together). Despite the prevalence of this mosaic transformation,
²⁴ estimated to occur in at least one quarter of all vertebrates, the cellular mechanisms that
²⁵ guide it have not been explored. There are currently no published mathematical models of
²⁶ this mosaic transformation. Here, I show that this transformation can arise by minimizing
²⁷ a loss function of the positions of cones. The simulated square mosaics achieve similar reg-
²⁸ ularity to mosaics observed in nature. The results suggest that square mosaics can arise
²⁹ from maximizing contacts between double cones and a certain class of single cones and
³⁰ maintaining a minimum separation between cones in that class.

³¹

³² 1 Introduction

³³ The cone photoreceptors of the vertebrate retina are specialized neurons that absorb light
³⁴ and transduce it into electrical signals, providing a pixel-like representation of the outside
³⁵ world that the brain interprets as visual imagery [1, 2]. Cones vary in biochemical and
³⁶ morphological attributes that determine their physiological and optical properties. This
³⁷ includes the main type of visual pigment expressed, a molecular complex consisting of a
³⁸ protein (opsin) covalently bound to a vitamin A-derived chromophore. Because of opsin
³⁹ and chromophore diversity, this complex can absorb maximally in either the ultraviolet
⁴⁰ (~320-400 nm), blue (~390-480 nm), green (~480-560 nm), or red (~540-630 nm) regions
⁴¹ of the human visual spectrum [3, 4]. Antagonistic interactions between cones expressing
⁴² different visual pigments provide the basis for colour vision [1, 5].

⁴³ Morphologically, there are three major types of cones: singles, doubles, and triples [6, 7].
⁴⁴ Single cones are individual cells with circular cross-section, whereas double and triple cones
⁴⁵ consist of two or three conjoint cells, respectively, and exhibit either elliptical (double cone)
⁴⁶ or quasi-triangular (triple cone) cross-sections at the level of the cells' somas [6]. The types
⁴⁷ and distributions of cones in vertebrate retinas vary widely with single cones present in all
⁴⁸ diurnal vertebrates and double and triple cones absent in eutherian mammals [8].

⁴⁹ Cones are distributed in mosaics of varying regularity over the retinal surface. In eu-
⁵⁰ therian mammals, single cones are patterned in hexagonal formation, where each cone is
⁵¹ surrounded on average by six neighbours [9], as in the human fovea [10, 11]. This is also
⁵² the case for the larval (pre-metamorphic) stages of all marine fishes that have been stud-
⁵³ ied [8, 12, 13, 14]. Double and, sometimes, triple cones are present in the adult retinas
⁵⁴ of vertebrates that are non-eutherian mammals (i.e., fishes, amphibians, reptiles, birds,
⁵⁵ monotremes, and marsupials) [7, 15]. In teleost (bony) fishes and some reptiles (geckos),
⁵⁶ single and double cones form highly regular, lattice-like mosaics, the most prevalent being
⁵⁷ the square mosaic where each single cone is surrounded by four double cones [6, 16]. An
⁵⁸ exception to this pattern is the row mosaic of zebrafish, *Danio rerio*, which consists of al-
⁵⁹ ternating rows of singles and double cones [17]. Lattice-like mosaics are believed to improve
⁶⁰ all aspects of visual function, such as colour discrimination, spatio-temporal acuity, and
⁶¹ feature detection [1, 18]. The fact that most retinal cell types and their brain targets ex-
⁶² hibit regularity in their patterning indicates its importance in processing visual information
⁶³ [19, 20].

⁶⁴ Over half of the world's vertebrate species are fishes (> 32,000) and, of these, about
⁶⁵ 57% are marine (as opposed to freshwater dwelling) [21]. Most fishes undergo some form
⁶⁶ of metamorphosis, a physiological process whereby the larva transforms into a juvenile.
⁶⁷ In marine fishes, this process involves the retinal transformation from a hexagonal cone
⁶⁸ mosaic to a square mosaic of varying regularity [8, 12, 13, 14, 22, 23, 24]. Because no new
⁶⁹ cones are generated during this life transition [12, 25], the single cones of the hexagonal

70 mosaic must transform into a square mosaic through a combination of coalescence (to form
71 double cones) and re-positioning. The cellular patterning rules required to guide such re-
72 arrangement have not been determined. Mathematical modeling of cone mosaic formation
73 based on biological observations has only been carried out for zebrafish to elucidate how the
74 adult mosaic forms at the retinal periphery [26, 27]. Any changes in the larval mosaic prior
75 to the appearance of the adult mosaic [17] remain unknown. The only modelling studies of
76 square mosaic formation examined another fish, the medaka (*Oryzias latipes*), and started
77 with the unrealistic initial condition of a randomly-distributed population of double and
78 single cones bound to a square lattice [28, 29]. Not only is this pattern never observed in
79 medaka, for which the square mosaic is present from hatching and expands as new cells
80 proliferate at the retinal margin [30], but it is also not observed in marine fishes. As such,
81 our understanding of the rules that may govern cone mosaic formation are restricted to the
82 adult mosaic of one species (the zebrafish) which is not representative of other fishes.

83 This thesis develops a computational model which transforms the hexagonal mosaics of
84 two marine fishes, sablefish (*Anoplopoma fimbria*) and Atlantic halibut (*Hippoglossus hip-*
85 *poglossus*), into square mosaics. The simulated square mosaics are quantitatively similar to
86 those observed in nature, as assessed by measures of cellular patterning and spatial regular-
87 ity. The results indicate that square mosaics can arise from maximizing contacts between
88 double cones and a certain class of single cones and maintaining a minimum separation
89 between cones in that class.

90 **2 Methodology**

91 **2.1 Model Description**

92 I propose an off-lattice computational model of the transformation from hexagonal to square
93 mosaic. The model is informed by biological observations of two marine fishes, Atlantic
94 halibut and sablefish, which exhibit the typical hexagonal to square mosaic transformation
95 observed in all marine fishes that have been examined and, potentially, in most freshwater
96 fishes as well [8]. The model expands upon the *overlapping spheres* paradigm of modelling
97 multicellular tissues [31, 32], which has been used to model tumour growth and intestinal
98 crypts [33, 34]. In this paradigm, each cell is modelled as a sphere of fixed radius, and cells
99 whose centres are within a given distance interact with one another. Cells move as a result
100 of these interactions and are not bound to a lattice.

101 In the present model, cells move to fulfill a set of objectives. These objectives avoid
102 making assumptions about the molecular mechanisms that underlie them. Each objective,
103 i , is realized as a real-valued function, f_i , of the positions of each cone, where mosaic
104 arrangements that fulfill or nearly fulfill the objective attain lower values and arrangements
105 which don't attain higher values. The *loss*, f , is the sum $f = \sum_i f_i$. The *mosaic induced by*

106 f is taken to be the arrangement of cones which minimizes f subject to a set of constraints,
107 as identified by a numerical optimization algorithm.

108 My model simulates a two-dimensional tangential cross section of the retina at the
109 level of cone inner segments. Single cones are modelled as discs, consistent with the shape
110 observed in tangential cross sections [6]. Double cones are modelled as the union of two
111 discs whose centres are at a fixed distance, d_{DC} , similar to the shape of a Venn diagram.
112 The cross sections of double cones may be better approximated with ellipses [6], but my
113 model uses discs to simplify the underlying mathematics. My model neglects triple cones, as
114 they are absent in perfect square mosaics, where “perfect” refers to an idealized, spatially
115 periodic mosaic. Figure 1 depicts a perfect square mosaic. The design of my model is guided
116 by the geometry of the perfect square mosaic.

117 Perfect mosaics are never observed in nature, though some fish mosaics are extremely
118 regular [6]. Conversely, micrographs of square mosaics in Atlantic halibut and sablefish
119 demonstrate many deviations from the perfect square mosaic (Figure 2). My model will be
120 considered successful if it generates mosaics similar to those observed in these two species,
121 as assessed by the regularity of patterning within and between cone types.

122 Each cone is assigned a unique identifier, i . The set of single cone identifiers is denoted
123 C_{SC} ; the set of double cones (i, j) consisting of cone i and cone j is denoted C_{DC} . The
124 position of cone i is the centre $\mathbf{r}_i = (x_i, y_i)$ of its corresponding disc. The position of a
125 double cone, (i, j) , is the centroid $\mathbf{r}_{ij} = (x_{ij}, y_{ij})$ of the union of the corresponding discs
126 for its two members. In other words, the position of (i, j) is $\mathbf{r}_{ij} = (x_i + x_j, y_i + y_j)/2$. The
127 angle, θ_{ij} , of the double cone (i, j) is the angle between the positive x -axis and the vector
128 $\mathbf{r}_i - \mathbf{r}_{ij}$. Hence, we may write \mathbf{r}_i and \mathbf{r}_j as in equations (1) and (2), respectively.

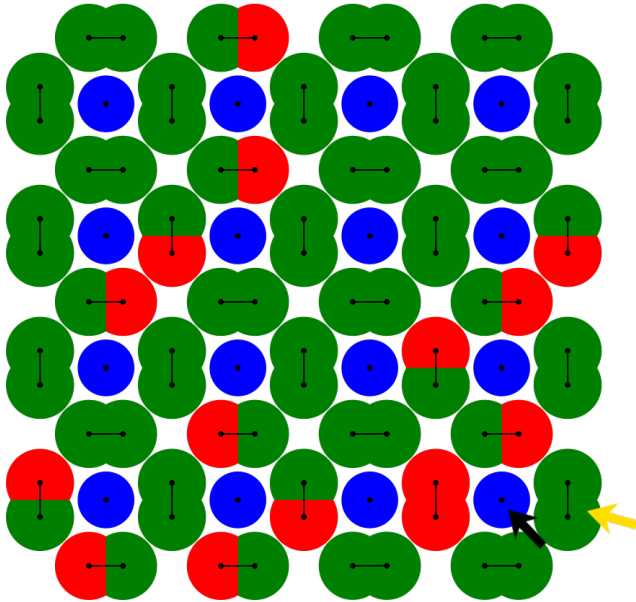
$$\mathbf{r}_i = \mathbf{r}_{ij} + \frac{d_{DC}}{2}(\cos(\theta_{ij}), \sin(\theta_{ij})) \quad (1)$$

$$\mathbf{r}_j = \mathbf{r}_{ij} - \frac{d_{DC}}{2}(\cos(\theta_{ij}), \sin(\theta_{ij})) \quad (2)$$

130 The discs that represent single cones are assumed to have the same diameter, D_{SC} ,
131 which is nondimensionalized to 1. D_{DC} , the diameter of each double cone member, is set
132 to 1.2, in accordance with the ratio $D_{DC} : D_{SC}$ observed in the centro-ventral retina of the
133 Atlantic halibut 103 days postfertilization (obtained by digitally measuring $N = 40$ pairs
134 of single and double cones in Figure 2B; mean \pm SD = 1.2 ± 0.2). d_{DC} is set to 0.6, such
135 that the ratio of each double cone’s length to its width, $(D_{DC} + d_{DC})/D_{DC}$, agrees with
136 that observed in the centro-ventral retina of the Atlantic halibut 103 days postfertilization
137 (obtained by digitally measuring $N = 10$ double cones in Figure 2B; mean \pm SD = $1.5 \pm$
138 0.2).

139 The input parameters for the objectives are \mathbf{r}_i for each single cone, i , and \mathbf{r}_{ij} and θ_{ij} for
140 each double cone, (i, j) . Since cones are anchored in place at their synaptic pedicles, they

Perfect Square Mosaic



Square Unit

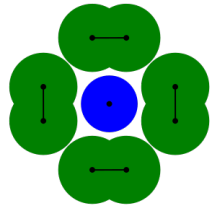


Figure 1: Isolated discs (black arrow) denote single cones, whereas pairs of overlapping discs (yellow arrow) denote double cones. The black dot within each cone denotes its centre, and a line between two cones indicates that they form a double cone. Each cone's spectral phenotype corresponds to its colour in the schematic. Left: A schematic of a *perfect square mosaic*, viewed tangential to the retinal surface. Each single cone is flanked by four double cones. The pattern continues in a spatially periodic fashion across the plane. Each double cone consists of some combination of green and red cones; the model treats both colours identically. All the centre cones are blue in the schematic, but green and red centre cones may also occur. Right: A *square unit*, a repeating motif in the perfect square mosaic. Square units consist of a central single cone flanked by four double cones.

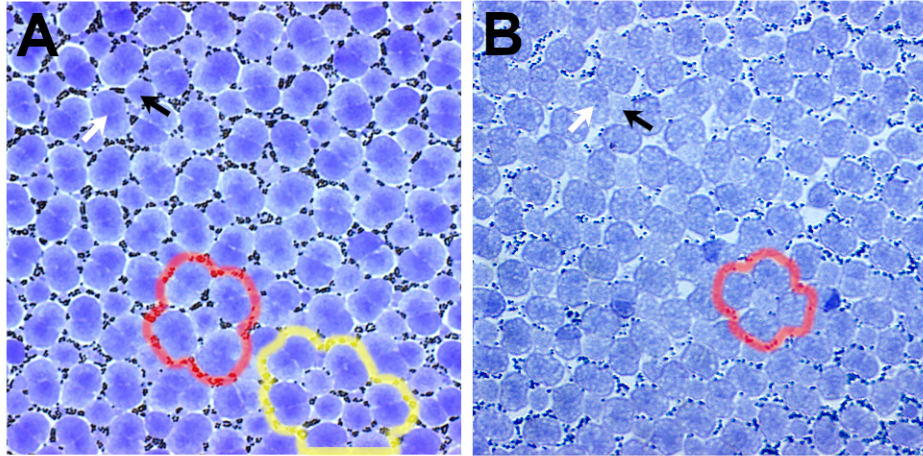


Figure 2: Micrographs of tangential EPON sections of sablefish and Atlantic halibut retinas at the level of the inner segments. (A) depicts a square mosaic in the sablefish retina. (B) depicts a square mosaic in the Atlantic halibut retina (reproduced from [23] with permission). Black arrows point to single cones, and white arrows point to double cones. Red highlights outline examples of square units. The yellow highlight outlines a cluster of single cones flanked by double cones.

141 are unable to move tangentially in the retinal plane in their entirety after synaptogenesis
 142 [35]. However, in retinal sections, cones are seen displaced laterally from their synaptic
 143 pedicles by tilting along their axons [23]. This displacement appears as a translation of cone
 144 inner segments in tangential cross sections. My model assumes that this lateral displacement
 145 underlies the spatial transformation necessary for square mosaic formation. Axons may only
 146 tilt so far, however, and the resultant limits on translation are implemented as bounds on
 147 each \mathbf{r}_i and \mathbf{r}_{ij} . If $(x_{i,0}, y_{i,0})$ is the position of a single cone, i , at the start of the simulation,
 148 then the constraints on the position of cone i are given by equations (3) and (4). The initial
 149 position of a double cone, (i, j) , is the mean of the initial positions of its constituent cones,
 150 and the constraints on \mathbf{r}_{ij} are as in equations (5) and (6). δ denotes the maximum distance
 151 that a cone may shift from its initial position along each coordinate axis.

$$x_{i,0} - \delta \leq x_i \leq x_{i,0} + \delta \quad (3)$$

$$y_{i,0} - \delta \leq y_i \leq y_{i,0} + \delta \quad (4)$$

$$\frac{x_{i,0} + x_{j,0}}{2} - \delta \leq x_{ij} \leq \frac{x_{i,0} + x_{j,0}}{2} + \delta \quad (5)$$

$$\frac{y_{i,0} + y_{j,0}}{2} - \delta \leq y_{ij} \leq \frac{y_{i,0} + y_{j,0}}{2} + \delta \quad (6)$$

155 The first objective, f_1 , which transcends mosaic geometry, is to prevent the excessive
 156 overlap of adjacent cones which are not both members of the same double cone. Inner
 157 segments of adjacent single cones have been observed to press against one another without

forming a double cone [8], analogous to discs intersecting in my model. Conversely, this objective prevents the non-physical behaviour of two discs overlapping substantially. f_1 is as in equation (7), which increases “punishment” (greater values of the loss function) as overlap increases, with no punishment in the absence of overlap. The auxiliary function, $g(d, r_1, r_2)$, in equation (8) dictates the punishment for overlap between a cone of radius r_1 and a cone of radius r_2 at a Euclidean distance of d . g is selected solely for its qualitative properties, and informal tests with qualitatively similar choices of g yielded similar behaviour. In equation (8), H is the Heaviside step function.

$$\begin{aligned}
 f_1(\mathbf{x}) = & \sum_{i \in C_{SC}} \sum_{\substack{j \in C_{SC}, \\ j > i}} g(\|\mathbf{r}_i - \mathbf{r}_j\|, D_{SC}/2, D_{SC}/2) \\
 & + \sum_{i \in C_{SC}} \sum_{(j,k) \in C_{DC}} g(\|\mathbf{r}_i - \mathbf{r}_j\|, D_{SC}/2, D_{DC}/2) + g(\|\mathbf{r}_i - \mathbf{r}_k\|, D_{SC}/2, D_{DC}/2) \\
 & + \sum_{(i,j) \in C_{DC}} \sum_{\substack{(k,l) \in C_{DC}, \\ k > i}} g(\|\mathbf{r}_i - \mathbf{r}_k\|, D_{DC}/2, D_{DC}/2) + g(\|\mathbf{r}_j - \mathbf{r}_l\|, D_{DC}/2, D_{DC}/2) \\
 & + \sum_{(i,j) \in C_{DC}} \sum_{\substack{(k,l) \in C_{DC}, \\ k \neq i}} g(\|\mathbf{r}_i - \mathbf{r}_l\|, D_{DC}/2, D_{DC}/2)
 \end{aligned} \tag{7}$$

$$g(d, r_1, r_2) = 10(r_1 + r_2 - d)^2 H(r_1 + r_2 - d) \tag{8}$$

In each simulation run, the positions and spectral phenotypes of cones were initialized from a micrograph of either the sablefish or the Atlantic halibut hexagonal mosaic. The spectral phenotypes of cones were determined from the main visual pigments they express [3, 22]. This thesis uses two initial conditions derived from micrographs of the Atlantic halibut and one initial condition derived from the sablefish, abbreviated AH1, AH2, and Sab, respectively (Figure 3A,B,C). All three initial conditions consist of red, green, and blue single cones but no ultraviolet cones.

The design of this model is guided by the geometry of the perfect square mosaic, as illustrated in Figure 1. A perfect square mosaic is a spatially periodic pattern consisting of *square units* tiling the Cartesian plane (in reality, the retinal surface is curved, but this model approximates it as locally planar). A square unit is a single cone, termed *centre cone*, that is flanked by four double cones, as depicted in Figure 1. In this model, the members of double cones may only be green or red, since blue cones do not occur as double cone members in Atlantic halibut or sablefish [23]. Blue cones are centre cones, but non-blue single cones can also serve as centre cones if blue cones are sparse, as observed in Atlantic halibut [23]. Sab contains enough blue cones to construct a square mosaic purely with blue centre cones, but blue cones are too sparse in AH1 and AH2 to do so. As the perfect square mosaic exhibits a ratio of four double cone members to one centre cone, this model

185 partitions the cones into two sets at the beginning of the simulation, S_{ND} and S_D , where
186 $|S_D| : |S_{ND}| = 4 : 1$. S_{ND} is the set of cones which may not form double cones, or “non-
187 doublable cones”. S_{ND} includes all blue cones and possibly some subset of non-blue cones
188 to achieve the 4:1 ratio. S_D is the set of cones which may be paired into double cones, or
189 “doublable cones”.

190 Since the square mosaic is assembled gradually in sablefish and Atlantic halibut, with
191 different retinal regions simultaneously exhibiting different stages of mosaic development
192 [8, 22, 23], my model emulates this behaviour. The *development rate*, σ , mediates the rate at
193 which the square mosaic is assembled. Each simulation run consists of a series of iterations.
194 In each iteration, the *double cone domain*, a circular domain in the centre of the simulation
195 space in which double cones are permitted to form, is expanded radially by a step of σ .
196 Then, new double cones are permitted to form within the double cone domain. Finally, the
197 current mosaic is updated to the mosaic induced by f . The simulation begins with a double
198 cone domain of radius zero and terminates after all cones are contained within the double
199 cone domain.

200 In each iteration, two single cones, i and j , are permitted to form a double cone if they
201 satisfy the following criteria:

- 202 • $i, j \in S_D$.
- 203 • i and j can attain a Euclidean distance of d_{DC} . More precisely, if

$$\sqrt{(\max(|x_{i,0} - x_{j,0}| - 2\delta, 0))^2 + (\max(|y_{i,0} - y_{j,0}| - 2\delta, 0))^2} \leq d_{DC}$$

204 This condition ensures that double cones only form between cones that can come in
205 close enough proximity to do so.

- 206 • Both i and j are within the current double cone domain.

207 To minimize assumptions about the pairs of single cones that form double cones and the
208 order in which double cones form, pairs of cones satisfying the above conditions are selected
209 uniformly at random to be paired. In each iteration, pairing stops once there are no longer
210 any pairs of single cones that satisfy the conditions.

211 An additional objective, f_2 , is needed to characterize the square mosaic pattern. Centre
212 cones are often not in contact with all four neighbouring double cones in tangential cross
213 sections, even if they may be in contact at other depths in the retina [8]. Since my model
214 simulates a tangential cross section at the level of cone inner segments, it aims to reproduce
215 the intercellular distances observed at this level in tangential micrographs of square mosaics,
216 neglecting distance information at other retinal depths.

217 By digitally measuring $N = 40$ pairs of single and double cones in a tangential cross
218 section of the square mosaic in the centro-ventral Atlantic halibut retina, I concluded that,

219 on average, a centre cone is at a distance of 1.2 times its diameter from the members of
 220 surrounding double cones (obtained from Figure 2B; mean \pm SD = 1.2 ± 0.2).

221 Geometry reveals that for the chosen D_{SC} , D_{DC} , and d_{DC} , the maximum number of
 222 double cone members which can simultaneously attain a distance of 1.2 from a given single
 223 cone without double cones overlapping is eight—precisely the number attained by a square
 224 unit. A natural objective, then, would be to maximize the number of pairs of non-doublable
 225 cones and double cone members which are at a distance of $d_{SD} = 1.2$ from one another.
 226 Establishing distances of 1.2 between cones may seem arbitrary, but this distance may
 227 represent contact between cones at other retinal depths. f_2 , as in equation (9), implements
 228 this objective by providing an increasing “reward” (lower values of the loss function) as the
 229 distance between a non-doublable cone and a member of a double cone approaches d_{SD} ,
 230 with the maximum reward occurring at a distance of d_{SD} . The auxiliary function $h(d)$ in
 231 equation (10) computes this reward as a function of the distance, d , between a non-doublable
 232 cone and a double cone member. Like g , h is chosen solely for its qualitative properties,
 233 and informal testing with qualitatively similar choices of h yielded similar performance. The
 234 auxiliary function u prevents interactions between non-doublable cones and double cones at
 235 unrealistic distances. The model considers interactions between a non-doublable cone and
 236 a double cone only if the domains in which the cones may exist overlap. u also enforces
 237 the gradual formation of the new mosaic by only considering interactions involving non-
 238 doublable cones whose original position lies within the current double cone domain. To be
 239 precise, for a non-doublable cone, i , and a double cone, (j, k) , $u(i, j, k) = 1$ if

$$[x_{i,0} - \delta, x_{i,0} + \delta] \times [y_{i,0} - \delta, y_{i,0} + \delta]$$

240 overlaps with

$$\left[\frac{x_{j,0} + x_{k,0}}{2} - \delta, \frac{x_{j,0} + x_{k,0}}{2} + \delta \right] \times \left[\frac{y_{j,0} + y_{k,0}}{2} - \delta, \frac{y_{j,0} + y_{k,0}}{2} + \delta \right]$$

241 and $(x_{i,0}, y_{i,0})$ is within the current double cone domain; $u(i, j, k) = 0$ otherwise.

$$f_2(\mathbf{x}) = \sum_{i \in S_{ND}} \sum_{(j,k) \in C_{DC}} u(i, j, k) (h(||\mathbf{r}_i - \mathbf{r}_j||) + h(||\mathbf{r}_i - \mathbf{r}_k||)) \quad (9)$$

$$h(d) = \frac{-1/5}{(15(d - d_{SD}))^2 + 1} \quad (10)$$

242 Initial tests using the Sab initial condition with $\delta = 2$ and $\sigma = 1$ were successful in gener-
 243 ating square units. However, many of the resultant mosaics featured clusters of blue cones
 244 surrounded by double cones (Figure 4). Such arrangements may be local optima of the loss
 245 function, but they are not characteristic of the perfect square mosaic. Clusters of single
 246 cones surrounded by double cones sometimes occur in retinal square mosaics, as demon-
 247 strated by the results of the simulations.

248 strated by Figure 2A, but not as frequently as they occurred in the simulations. Outside of
 249 clusters, many simulated mosaics also exhibited pairs of blue cones with insufficient intercel-
 250 lular distances to fit double cones between them. Conversely, separation between blue cones
 251 is pervasive in the premetamorphic hexagonal mosaics of Atlantic halibut and sablefish,
 252 wherein two blue cones are never observed to be adjacent [23]. Therefore, I postulate that
 253 there is a mechanism which maintains separation between blue cones during metamorphosis.

254 To induce a separation between blue cones, and, more generally, between non-doublable
 255 cones, I introduce another objective, f_3 , which punishes pairs of non-doublable cones whose
 256 distance falls below a given minimum, μ . f_3 is as in equation (11), and it increases sharply
 257 as the distance between two non-doublable cones falls below μ and provides a negligible
 258 punishment for non-doublable cones at a distance greater than μ . The auxiliary function
 259 $l(d)$ in equation (12) computes this punishment as a function of the distance, d , between
 260 two non-doublable cones. Like the other auxiliary functions, l is chosen purely for its qual-
 261 itative properties, and informal testing with qualitatively similar choices of l yielded similar
 262 behaviour. Like u , the auxiliary function v enforces the gradual formation of the new mosaic
 263 by only permitting interactions between non-doublable cones whose original positions lie
 264 within the double cone domain. More precisely, for $i, j \in S_{ND}$, $v(i, j) = 1$ if $(x_{i,0}, y_{i,0})$ and
 265 $(x_{j,0}, y_{j,0})$ are within the current double cone domain; otherwise, $v(i, j) = 0$.

$$f_3(\mathbf{x}) = \sum_{i \in S_{ND}} \sum_{\substack{j \in S_{ND}, \\ j > i}} v(i, j) l(||\mathbf{r}_i - \mathbf{r}_j||) \quad (11)$$

$$l(d) = 10e^{-30(d + \frac{1}{5} - \mu)} \quad (12)$$

266 The model must select some non-blue cones to be non-doublable cones for AH1 and
 267 AH2, as both exhibit too few blue cones to attain a ratio of $|S_D| : |S_{ND}| = 4 : 1$ using
 268 only blue cones as non-doublables. Since no two blue cones are adjacent in any of the
 269 initial conditions, the non-blue cones which are selected as non-doublables may also exhibit
 270 a minimum separation in the initial condition. The parameter τ represents the minimum
 271 permitted distance between any two non-doublable cones in the initial condition. The model
 272 selects a subset of non-blue cones to be non-doublables of a cardinality large enough to
 273 achieve a ratio of $|S_D| : |S_{ND}| = 4 : 1$, while ensuring that each pair of cones in S_{ND} is at a
 274 distance of at least τ . This subset of non-blue cones is selected uniformly at random among
 275 all subsets of the required cardinality that satisfy the distance constraints.
 276

277 2.2 Simulations

278 Each of δ , σ , and μ was varied over a representative range for the one sablefish initial
 279 condition and two Atlantic halibut initial conditions; τ was also varied for the Atlantic
 280 halibut initial conditions. Model parameters and their assigned values are summarized in
 281 Table 1.

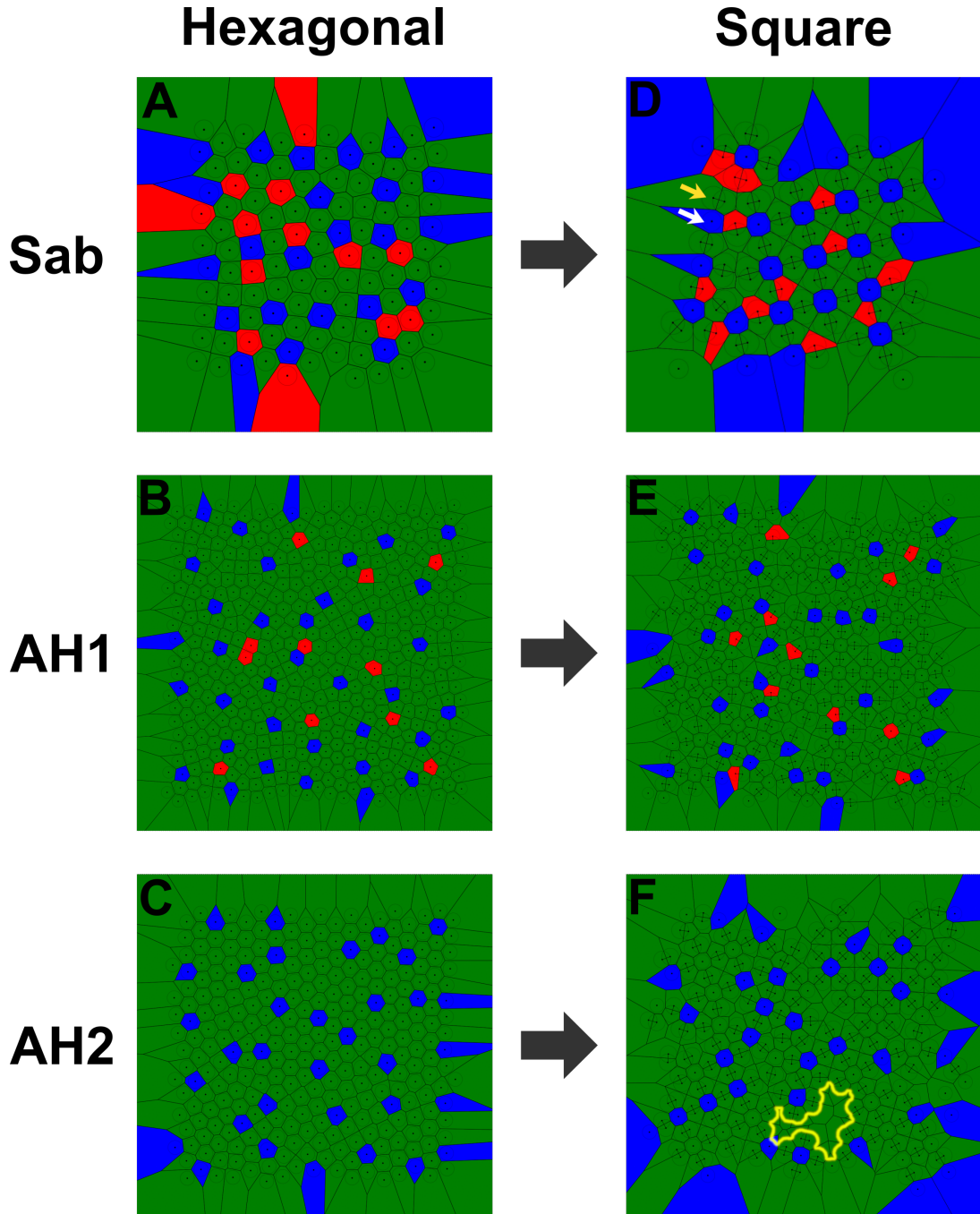


Figure 3: Left column: Schematics of the Sab (A), AH1 (B), and AH2 (C) initial conditions. Right column: Mosaics generated by the best performing parameter set for Sab (D), AH1 (E), and AH2 (F). The white arrow points to a single cone, and the yellow arrow points to a double cone. The perimeter of each cone is denoted by a grey circle, and the centre of each cone is denoted by a black dot. A line adjoining the centres of two cones indicates that they form a double cone. A Voronoi tessellation generated from the cell centres is superimposed on the mosaics as a visual aid, where each Voronoi cell is outlined in black. The spectral phenotype of a cone is denoted by the colour of its Voronoi cell. The yellow highlight in (F) indicates a region in the mosaic that was populated with cones in the initial condition but had become empty by the end of the simulation.

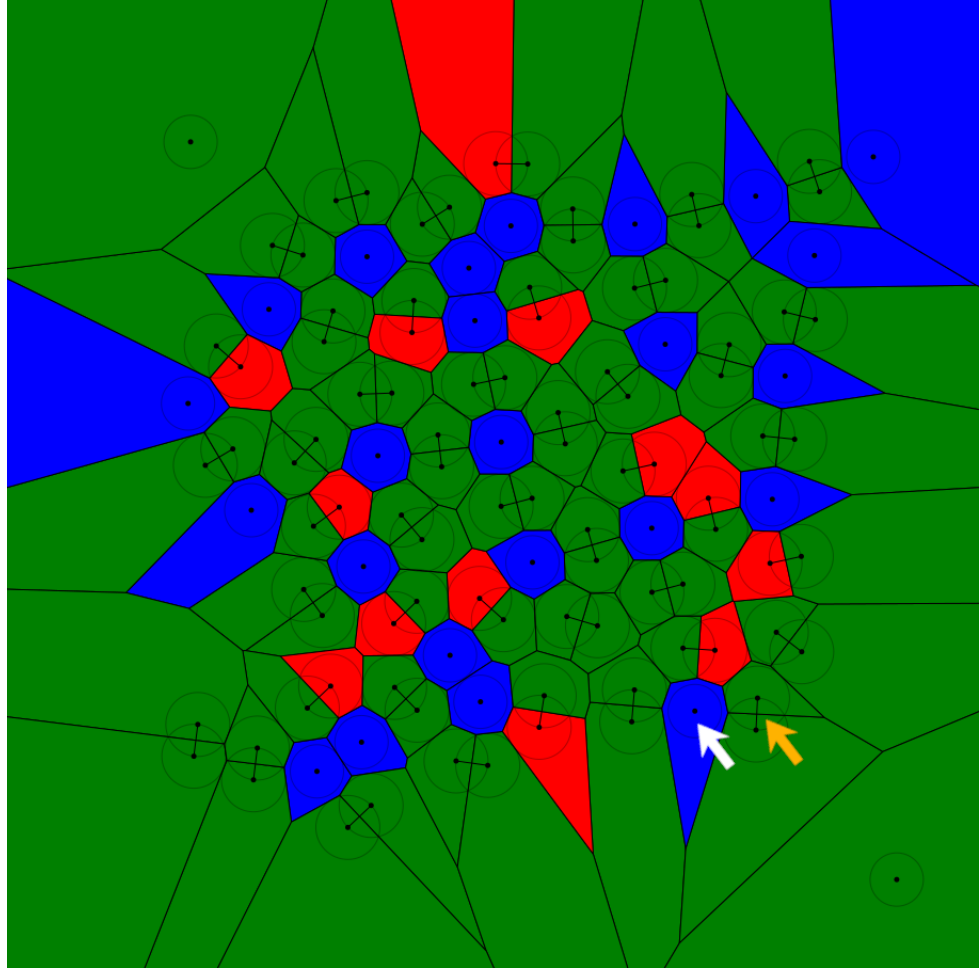


Figure 4: A schematic generated from the Sab initial condition using $\delta = 2$ and $\sigma = 1$, before the implementation of separation between non-doublable cones. The white arrow points to a single cone, and the yellow arrow points to a double cone. The perimeter of each cone is denoted by a grey circle, and the centre of each cone is denoted by a black dot. A line adjoining the centres of two cones indicates that they form a double cone. A Voronoi tessellation generated from the cell centres is superimposed on the mosaic as a visual aid, where each Voronoi cell is outlined in black. The spectral phenotype of a cone is denoted by the colour of its Voronoi cell. The schematic exhibits several clusters of blue cones surrounded by double cones. Such clusters occur consistently in simulations in the absence of an induced separation between non-doublable cones.

282 For each Atlantic halibut initial condition and each parameter assignment, five simulation
283 runs were conducted using different random seeds. 20 simulation runs were conducted
284 for the sablefish initial condition due to their quicker compute times. The loss function was
285 minimized using the L-BFGS-B implementation in JAXopt version 0.85 [36] with a tolerance
286 of 0.001 and a maximum of 10,000 iterations. Input parameters were bounded as in
287 equations (3), (4), (5), and (6).

288 The performance of a parameter set was measured using a custom metric henceforth
289 referred to as the *square mosaic score* (SMS). The square mosaic score relies upon the
290 observation that in a square unit, the line segment from the centre cone to the centre of
291 a neighbouring double cone is approximately perpendicular to the line segment from one
292 member of the double cone to the other. The SMS considers a single cone, j , to be the centre
293 cone of a valid square unit if for each of the four nearest double cones, (k_i, l_i) , $1 \leq i \leq 4$,
294 the angle between $\mathbf{r}_{k_i l_i} - \mathbf{r}_j$ and $\mathbf{r}_{k_i} - \mathbf{r}_{l_i}$ is within $\frac{\pi}{2} \pm \varepsilon$ radians for a given ε . I select $\varepsilon = 0.3$
295 based upon informal observations of the extent to which a square unit can be perturbed
296 and remain discernibly so.

297 It is unreasonable to expect all single cones to become centre cones of square units, since
298 some single cones are close to the edges of the simulation space. In this case, there may not
299 be a sufficient number of double cones in a single cone's vicinity for it to be engulfed by four
300 of them. To account for cones on the edges, the square mosaic score discounts any single
301 cones whose original position is within a distance of 2 of the margin, where the margin is
302 defined as the boundary of the axis-aligned minimum bounding box of the cone centres in
303 the initial condition.

304 The square mosaic score of a mosaic is the proportion of single cones which are the centre
305 cone of a valid square unit, discounting cones whose initial position is within a distance of
306 2 of the margin.

307 3 Results

308 Among the 90 parameter sets attempted for the sablefish and 360 attempted for the At-
309 lantic halibut, the five sets that achieved the greatest mean SMS are summarized by initial
310 condition in Table 2. To compare the performance of the simulations to retinal square mo-
311 saics, the SMS was computed for five micrographs of the Atlantic halibut square mosaic
312 and four micrographs of the sablefish square mosaic. The margin in which single cones are
313 discounted by the SMS was modified for these calculations; single cones within 75 pixels
314 of the edge of each image were discounted. The retinal Atlantic halibut mosaics achieved a
315 mean score of 0.53 ± 0.13 , whereas those of the sablefish obtained a mean score of $0.39 \pm$
316 0.07. The mean SMSs of the five parameter sets attaining the highest mean for each initial
317 condition were compared to the mean SMSs of their respective species' retinal mosaics us-
318 ing Welch's t -test. The resulting p -values are listed in Table 2. The mean SMSs of the top

Table 1: Summary of model parameters.

Parameter	Value(s)	Description
D_{SC}	1	Nondimensionalized diameter of a single cone.
D_{DC}	1.2	Diameter of a member of a double cone.
d_{DC}	0.6	Distance between the centres of the members of a double cone.
d_{SD}	1.2	Optimal distance between a centre cone and the members of surrounding double cones in a square unit.
δ	0.5, 1, 1.5, 2, 2.5, 3	Maximum distance a cone may travel from its starting position along each coordinate axis.
σ	1, 2, 3	Development rate (rate at which the new mosaic is assembled).
μ	0, 1.5, 2, 2.32379, 2.5	Minimum permitted distance between two non-doublable cones. 2.32379 is the least distance between centre cones in the perfect square mosaic.
τ	0, 1.5, 1.75, 2	Minimum permitted initial distance between any two non-doublable cones. Only for AH1 and AH2.

Table 2: Parameter sets which achieved the greatest mean square mosaic scores.

(a) Sab

Rank	δ	σ	μ	Square Mosaic Score Mean	Square Mosaic Score SD	p -value
1.	2.5	1	2.32379	0.56	0.17	0.009
2.	2	1	2.32379	0.52	0.23	0.06
3.	1.5	1	2.32379	0.49	0.22	0.12
4.	2	3	2.32379	0.42	0.18	0.51
5.	2.5	2	2.32379	0.42	0.22	0.65

(b) AH1

Rank	δ	σ	μ	τ	Square Mosaic Score Mean	Square Mosaic Score SD	p -value
1.	2.5	1	2.32379	2	0.43	0.03	0.18
2.	3	1	2.32379	2	0.41	0.07	0.13
3.	1.5	1	2.32379	2	0.38	0.04	0.07
4.	3	1	2.32379	1.75	0.38	0.12	0.11
5.	2	1	2.32379	2	0.38	0.07	0.06

(c) AH2

Rank	δ	σ	μ	τ	Square Mosaic Score Mean	Square Mosaic Score SD	p -value
1.	2.5	1	2.32379	1.5	0.51	0.06	0.74
2.	2.5	1	2.32379	1.75	0.47	0.10	0.47
3.	2	1	2.32379	2	0.42	0.16	0.28
4.	2.5	1	2.32379	2	0.42	0.14	0.23
5.	2.5	2	2.32379	1.5	0.41	0.07	0.14

319 five parameter sets for the Atlantic halibut initial conditions were not significantly different
 320 from the mean observed in Atlantic halibut retinas. For the sablefish, the best parameter
 321 set's mean score was significantly different from the mean observed in the retinal mosaics,
 322 whereas the other means were not. Mosaic schematics generated by the best parameter set
 323 for each initial condition are in Figure 3D,E,F.

324 I used the *Voronoi area regularity index* (VARI) as an additional means of comparing
 325 performance between simulated and retinal mosaics. The Voronoi area regularity index for
 326 a set of points is the mean area of each cell in the Voronoi tessellation of the points divided
 327 by the standard deviation of the areas, excluding any point whose Voronoi cell intersects
 328 with a chosen boundary. For an image of a mosaic, the boundary is the border of the image.
 329 For each run of the best performing parameter set for each initial condition, I computed the
 330 VARI for the centres of the single cones and the centres of the double cones. I computed
 331 the same metrics for the five retinal Atlantic halibut mosaics and four retinal sablefish
 332 mosaics. These results are summarized in Table 3. A high VARI indicates that points are

Table 3: VARI of retinal mosaics and the best parameter sets of simulated mosaics

(a) Retinal mosaics

Cone Type	Species	VARI Mean	VARI SD
Single	Sablefish	6.41	3.94
	Atlantic halibut	8.38	4.01
Double	Sablefish	9.63	1.76
	Atlantic halibut	12.25	4.06

(b) Simulated mosaics

Cone Type	Initial Condition	VARI Mean	VARI SD	p-value
Single	Sab	5.85	2.34	0.80
	AH1	5.39	0.83	0.17
	AH2	5.32	1.54	0.17
Double	Sab	6.02	1.31	0.02
	AH1	5.43	0.66	0.02
	AH2	5.52	0.39	0.02

333 distributed in a spatially regular fashion, so a high VARI for both single cones and double
 334 cones suggests that a mosaic is highly regular.

335 The mean VARI for the single cones of the best performing parameter set for Sab was not
 336 significantly different from the mean VARI of the single cones in the retinal sablefish mosaics.
 337 Likewise, the mean single cone VARIs for the best performing parameter sets of AH1 and
 338 AH2 were not significantly different from the mean VARI of the retinal Atlantic halibut
 339 mosaics. For all three initial conditions, however, the mean double cone VARIs for the best
 340 performing parameter sets were significantly different from those of the retinal mosaics.
 341 Indeed, for each initial condition, the mean double cone VARI was lower than that of the
 342 retinal mosaics. One likely cause of this discrepancy is the “holes” in simulated mosaics—
 343 that is, regions that were populated with cones in the initial condition but had become empty
 344 by the end of the simulation (Figure 3F). Excluding the optic disc, regions without cones
 345 are never observed in healthy retinas [37], but they are an issue that pervades my model.
 346 Typically, these regions are surrounded by square units of heterogeneous orientations, and in
 347 particular, the perimeters of the regions are lined with double cones. These bordering double
 348 cones have much larger Voronoi areas than the double cones in spatially regular regions.
 349 Potential solutions to this issue are proposed in the discussion section. The discrepancy
 350 in double cone VARIs notwithstanding, the similarities in single cone VARIs and SMSs
 351 suggest that this model is capable of generating square mosaics of similar regularity to
 352 those observed in nature.

353 **3.1 Parameter Analysis**

354 This section analyzes the parameters whose impact upon square mosaic formation is most
355 significant and the parameter ranges which best mediate square mosaic formation. For each
356 parameter and each assigned value, Figure 5 indicates the number of parameter sets with
357 that value assignment which attained a mean SMS of at least 1/3. The value assignments
358 which occur most frequently among these parameter sets are likely to be those that best
359 mediate square mosaic formation.

360 To supplement this analysis, for any one parameter with one fixed value, I computed the
361 mean of the square mosaic scores achieved by the simulations with that value assignment.
362 These means are summarized in Table 4. For each initial condition and each parameter,
363 I compared these means across all value assignments of the parameter. I used a one-way
364 ANOVA to determine if there were significant differences in mean SMSs between the value
365 assignments. If there were, which was the case for every parameter, I used Tukey's HSD to
366 determine which pairs of value assignments exhibit significantly different mean SMSs. Many
367 parameter sets yielded zero or near-zero square mosaic scores across all runs; to preserve
368 normality assumptions for hypothesis testing, I discounted from this analysis all parameter
369 sets for which fewer than the majority of runs yielded a positive SMS. For the sablefish
370 initial condition, there was no parameter set with $\delta = 0.5$ which attained a positive SMS in
371 the majority of runs; I therefore discounted the case of $\delta = 0.5$ from hypothesis testing for
372 the sablefish. The results of the ANOVA and Tukey's HSD are summarized in Figure 6.

373 **Analysis of δ**

374 Across all initial conditions, no parameter set with $\delta = 0.5$ attained a mean SMS of at least
375 1/3. For $\delta = 1$, two parameter sets surpassed this threshold for Sab, although none did for
376 the Atlantic halibut. All initial conditions had parameter sets with $\delta \geq 1.5$ that surpassed
377 this threshold.

378 For AH1 and AH2, $\delta = 0.5$ and $\delta = 1$ attained mean SMSs that were significantly differ-
379 ent from each other and from all other assignments of δ . In particular, $\delta = 0.5$ yielded means
380 that are strikingly lower than for other values of δ (Table 4B,C). In AH1, the differences
381 in mean performance between $\delta = 1.5$, 2, 2.5, and 3 were pairwise insignificant, with the
382 exception of $\delta = 1.5$ and $\delta = 2.5$, for which the difference was significant ($p = 0.01$); for
383 AH2, the differences in mean performance between $\delta = 1.5$, 2, 2.5, and 3 were all pairwise
384 insignificant. For the sablefish, $\delta = 0.5$ was neglected from hypothesis testing; its failure to
385 constitute a parameter set which achieved a mean SMS of at least 1/3 evidences that it
386 performs worse than the other values of δ . The differences in mean performance between
387 $\delta = 1$, 1.5, 2, 2.5, and 3 were pairwise insignificant for Sab, except for $\delta = 2.5$ and $\delta = 3$
388 ($p = 0.02$).

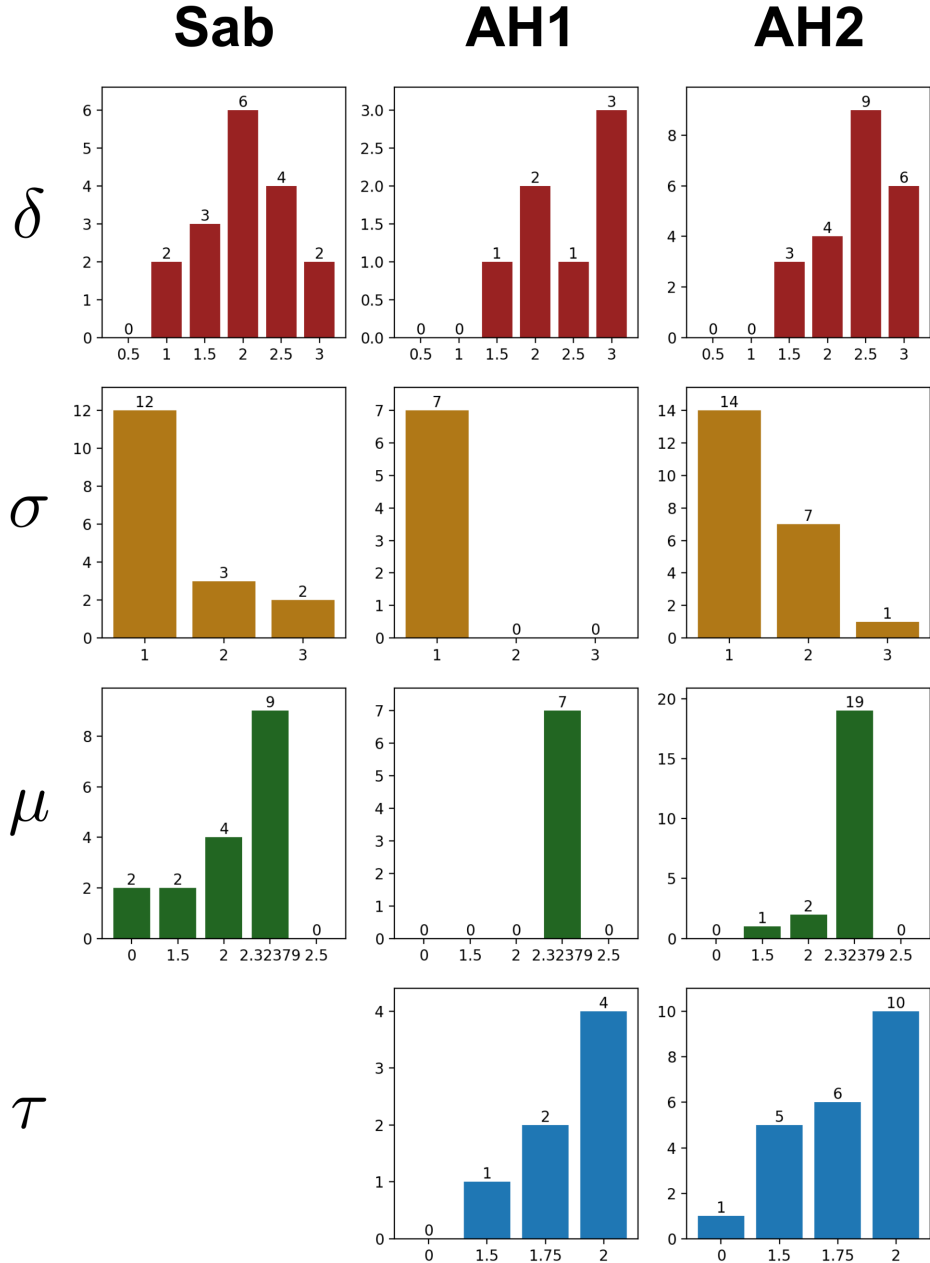


Figure 5: Counts of parameter sets which achieved a mean SMS of at least $1/3$. The columns indicate initial conditions, and the rows indicate each of the four parameters that was varied across simulations. In the bar chart for initial condition x and parameter y , each bar indicates the number of parameter sets with a particular assignment of y that achieved a mean SMS of at least $1/3$ for x . The space in the Sab column and τ row is vacant because τ is not a parameter for the sablefish initial condition.

Table 4: Mean SMS for each parameter assignment

(a) Sab

Parameter	Square Mosaic Score (Mean \pm SD)					
	0.5	1	1.5	2	2.5	3
δ	0.5	1	1.5	2	2.5	3
	N/A	0.25 ± 0.16	0.27 ± 0.18	0.27 ± 0.20	0.29 ± 0.21	0.24 ± 0.17
σ	1	2	3			
	0.30 ± 0.21	0.25 ± 0.17	0.24 ± 0.17			
μ	0	1.5	2	2.32379	2.5	
	0.24 ± 0.16	0.27 ± 0.16	0.30 ± 0.18	0.38 ± 0.20	0.098 ± 0.086	

(b) AH1

Parameter	Square Mosaic Score (Mean \pm SD)					
	0.5	1	1.5	2	2.5	3
δ	0.012 ± 0.011	0.13 ± 0.07	0.17 ± 0.09	0.19 ± 0.10	0.19 ± 0.10	0.19 ± 0.10
σ	1	2	3			
	0.19 ± 0.11	0.14 ± 0.10	0.14 ± 0.08			
μ	0	1.5	2	2.32379	2.5	
	0.17 ± 0.08	0.17 ± 0.08	0.18 ± 0.08	0.21 ± 0.12	0.048 ± 0.031	
τ	0	1.5	1.75	2		
	0.13 ± 0.08	0.15 ± 0.10	0.16 ± 0.11	0.19 ± 0.11		

(c) AH2

Parameter	Square Mosaic Score (Mean \pm SD)					
	0.5	1	1.5	2	2.5	3
δ	0.018 ± 0.016	0.16 ± 0.09	0.20 ± 0.11	0.21 ± 0.12	0.22 ± 0.13	0.21 ± 0.12
σ	1	2	3			
	0.22 ± 0.13	0.19 ± 0.11	0.17 ± 0.10			
μ	0	1.5	2	2.32379	2.5	
	0.20 ± 0.09	0.20 ± 0.10	0.22 ± 0.10	0.28 ± 0.14	0.069 ± 0.043	
τ	0	1.5	1.75	2		
	0.16 ± 0.11	0.19 ± 0.11	0.20 ± 0.12	0.21 ± 0.13		

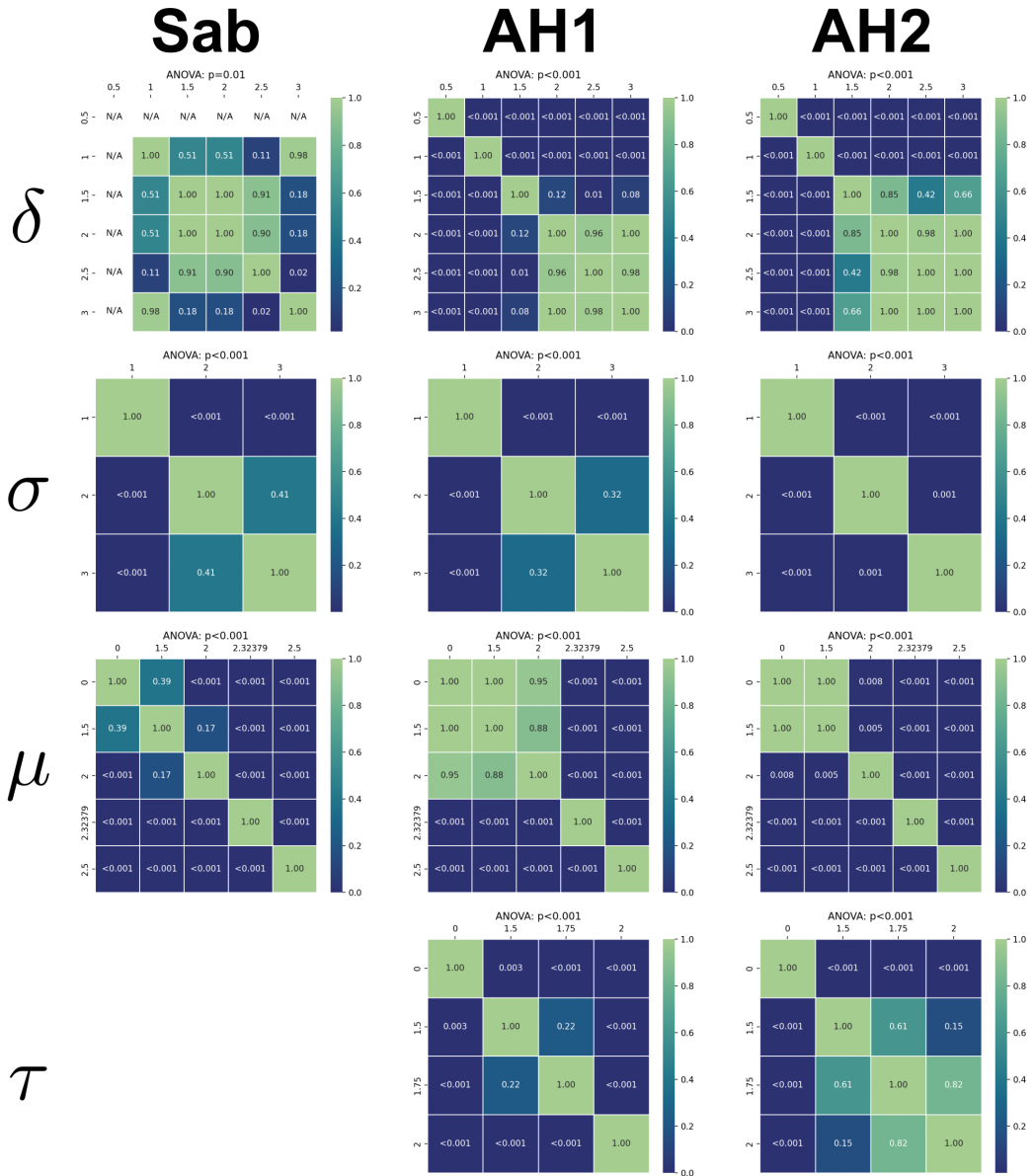


Figure 6: Heatmaps quantifying the significance of the difference in mean SMS between varying assignments of each parameter. The columns indicate initial conditions, and the rows indicate each of the four parameters that was varied across simulations. For each initial condition x , parameter y , and value assignment k of y , the square mosaic scores of parameter sets of x with $y = k$ were compiled, neglecting any parameter sets for which fewer than the majority of runs achieved a positive SMS. A one-way ANOVA was conducted on these compiled SMSs for each x and y , and the resulting p -value is listed above the heatmap in column x and row y . Subsequently, Tukey's HSD was used to test for pairwise differences in mean SMS between distinct assignments, k and l , of y . The p -value for the difference in mean SMS between $y = k$ and $y = l$ for initial condition x and parameter y is provided in the row labelled k and column labelled l of the heatmap in row y and column x . N/A is written in the row and column corresponding to $\delta = 0.5$ for Sab because no parameter set with $\delta = 0.5$ achieved a positive SMS in the majority of runs.

389 In aggregate, these results suggest that for Atlantic halibut, cones must be able to shift
390 at least 1.5 single cone diameters along each axis to form moderately regular square mosaics,
391 with diminishing returns for greater values of δ . The cones of the sablefish need not move as
392 far to form the square mosaic; they only need to be able to shift one single cone diameter.
393 With only one sablefish initial condition, however, the reproducibility of this result remains
394 to be seen.

395 **Analysis of σ**

396 Across all initial conditions, there were more parameter sets with $\sigma = 1$ whose mean SMS
397 surpassed $1/3$ than there were for $\sigma > 1$. In AH1, neither $\sigma = 2$ nor $\sigma = 3$ yielded any
398 parameter sets meeting this threshold. For both Sab and AH1, the mean SMSs for $\sigma = 2$
399 and $\sigma = 3$ were not significantly different, while $\sigma = 1$ was different from both. For AH2,
400 all values of σ were pairwise significantly different in mean SMS. In all initial conditions,
401 $\sigma = 1$ constituted the top three best performing parameter sets.

402 In aggregate, these results suggest that while square mosaic formation is possible for
403 $\sigma > 1$, $\sigma = 1$ mediates mosaic formation more robustly and consistently. This trend is
404 consistent across both species under consideration. A physical interpretation of this result
405 is that the transitional band of cones separating the premetamorphic hexagonal mosaic and
406 the postmetamorphic square mosaic is relatively narrow, perhaps as narrow as one single
407 cone diameter.

408 **Analysis of μ**

409 The most frequent value of μ among parameter sets whose mean SMS surpassed $1/3$ was
410 $\mu = 2.32379$ in all initial conditions. In AH1, $\mu = 2.32379$ was the only value of μ to
411 attain this performance threshold. While a few parameter sets with $\mu < 2.32379$ crossed
412 this threshold in the other initial conditions, no parameter set with $\mu = 2.5$ ever did. In
413 all initial conditions, the mean SMSs of parameter sets with $\mu = 2.32379$ and $\mu = 2.5$ were
414 significantly different from those of all other μ ; the difference in means between $\mu = 2.32379$
415 and $\mu = 2.5$ was also significant in all initial conditions. In the sablefish, the mean SMSs
416 of $\mu = 0$ and $\mu = 1.5$ were not significantly different, nor were those of $\mu = 1.5$ and $\mu = 2$;
417 however, $\mu = 0$ and $\mu = 2$ achieved significantly different means. For AH1, the differences
418 in mean SMSs between $\mu = 0$, 1.5 , and 2 were pairwise insignificant. In AH2, the mean
419 SMSs of $\mu = 0$, 1.5 , and 2 were pairwise significantly different, with the exception of $\mu = 0$
420 and $\mu = 1.5$. In all three initial conditions, 2.32379 was the only value of μ present among
421 the five best performing parameter sets.

422 Taken together, these results suggest that in both sablefish and Atlantic halibut, pre-
423 serving a minimum separation between non-doublable cones is essential for forming square
424 mosaics. Moreover, the performance is highly sensitive to the value of μ : too low of a μ
425 performs similarly to having no minimum separation at all, whereas too high of a μ yields

even worse performance. Inspecting the mosaic schematics when $\mu = 2.5$ reveals that many blue cones are ejected to the margins of the mosaic, or even beyond the margins if δ so permits. Given the density of non-doublable cones, it may be difficult or even impossible to establish a minimum distance of 2.5 between them without exceeding the margins of the mosaic.

The results suggest that $\mu = 2.32379$ best mediates square mosaics. This is a natural choice of μ , as it represents the least distance between two centre cones in the perfect square mosaic for the chosen d_{DC} and d_{SD} . Once this distance is established between non-doublable cones, double cones need only slide between them to form square units. There may be more performant values of μ in the neighbourhood of 2.32379, but determining them would require a finer-grained analysis.

One physical interpretation of these results would be that as the new mosaic forms, a mechanism activates in non-doublable cones which establishes a minimum distance of around 2.32379. However, this minimum distance is nearly achieved between blue cones in the sablefish hexagonal mosaic: of the 276 unique pairs of blue cones, only nine exhibit a distance of less than 2.32379, the least of which being 2.09683. Moreover, the mean of the distances between each blue cone and its nearest neighbour is not significantly different from 2.32379 (mean \pm SD = 2.29 ± 0.13 , $p = 0.21$). Hence, in the sablefish, we may interpret a μ of 2.32379 as merely maintaining the minimum distance already enforced in the hexagonal mosaic. Indeed, the mechanism that induces a minimum separation in the hexagonal mosaic may also be responsible for maintaining this separation during metamorphosis. This interpretation does not apply immediately to AH1 or AH2, as we cannot know for certain the distance between non-blue non-doublable cones in the initial conditions; for a large enough τ , however, this same interpretation may apply.

Analysis of τ

In both Atlantic halibut initial conditions, each value of τ constituted at least one parameter set which attained a mean SMS of 1/3, with the exception of $\tau = 0$ in AH1. In both initial conditions, $\tau = 2$ occurred most frequently among parameter sets that reached this performance threshold. For AH1, the mean SMSs achieved by $\tau = 0$, 1.5, 1.75, and 2 were pairwise significantly different, with the exception of $\tau = 1.5$ and $\tau = 1.75$. As for AH2, the differences in mean SMSs between $\tau = 1.5$, 1.75, and 2 were pairwise insignificant, but each mean was significantly different from that of $\tau = 0$. Every value of τ except for zero appeared among the top five parameter sets of at least one initial condition.

Taken in aggregate, these results suggest that τ must be greater than zero to consistently and robustly generate square mosaics, even if it is sometimes possible to generate moderately regular square mosaics with $\tau = 0$. The extent to which performance improves, if at all, as τ increases beyond 1.5 is unclear. One interpretation of these results is that two non-doublable cones should not be neighbours in the initial condition, where “neighbour” could be defined

464 using the Delaunay tesselation. Indeed, the mean distances between neighbouring cones in
465 the Delaunay tesselation for AH1 and AH2 are 1.23 ± 0.16 and 1.22 ± 0.12 , respectively,
466 indicating that a distance of 1.5 is unlikely to occur between neighbouring cones. This
467 interpretation is consistent with the sablefish initial condition, in which no two blue cones
468 are neighbours in the Delaunay tesselation (after discounting cones on the convex hull).

469 4 Discussion

470 For a fastidious choice of objectives, this model is capable of transforming hexagonal mosaics
471 into square mosaics of comparable regularity to those observed in Atlantic halibut and
472 sablefish. The chosen objectives are not inherently sufficient to generate regular square
473 mosaics, however. An effective assignment of parameter values is also necessary for square
474 mosaic formation.

475 The results suggest that cones must be able to shift 1.5 single cone diameters along
476 each axis to form square mosaics of moderate regularity, although a shift of one single cone
477 diameter may be sufficient for the sablefish. A maximum shift of $\delta = 3$ single cone diameters
478 may be unrealistic, but shifts of 1.5 or 2 can be informally justified by inspecting Figure
479 2B,D,F of [23], wherein cones' axons are quite tilted and their inner segments are laterally
480 displaced from their pedicles.

481 Although performance is less sensitive to σ , square mosaic formation is more robust
482 for lower values of σ . The notion of a narrow band separating the hexagonal mosaic from
483 the square mosaic is consistent with micrographs of transitional regions of the retinas of
484 Atlantic halibut undergoing metamorphosis, wherein groups of quasi-square units are very
485 close to the hexagonal mosaic (see Figure 6A of [8]).

486 The results indicate that non-doublable cones should not be neighbours in the initial
487 condition. This is consistent with observations of the Atlantic halibut retina, wherein blue
488 cones are always surrounded by non-blue neighbours [23]. It is unknown, however, if this
489 spacing rule is enforced between non-blue cones that become centre cones.

490 The results suggest that there is a mechanism that maintains a J. Pathol. distance
491 of approximately 2.3 between non-doublable cones as the square mosaic forms. Without
492 this mechanism, non-doublable cones which are distant in the initial condition tend to
493 form clumps flanked by double cones. The results suggest that there is a mechanism that
494 maintains a minimum distance of approximately 2.3 between non-doublable cones as the
495 square mosaic forms. Without this mechanism, non-doublable cones which are distant in
496 the initial condition tend to form clumps flanked by double cones.

497 Analyzing the parameter settings which achieve the best performance elucidates a po-
498 tential developmental program for the transformation of hexagonal mosaics into square
499 mosaics. Such a program is as follows:

500 • The square mosaic is constructed in a gradually expanding domain by forming double
501 cones from proximate pairs of single cones of the desired spectral phenotypes (non-
502 blue, in this case).

503 • Double cones and non-doublable cones in the expanding domain shift and rotate to
504 maximize contact with one another.

505 • Non-doublable cones maintain a minimum distance. The minimum distance is enforced
506 passively, in that non-doublable cones are not neighbours in the initial condition; it
507 is also enforced actively, in that some mechanism maintains this separation as the
508 square mosaic assembles.

509 The notion of a gradually assembling square mosaic is well supported by spatiotem-
510 poral differences in the mosaic geometries of different retinal regions in marine fishes
511 [8, 12, 13, 14, 22, 23, 24]. There is no known mechanism which would maximize contacts
512 between double cones and non-doublable cones, although differential adhesion is often hy-
513 pothesized to bring about regular mosaics by favouring contact between specific types of
514 cones [28, 38, 39]. Likewise, it is unclear what mechanism would maintain a minimum dis-
515 tance between non-doublable cones. Homotypic spacing has been observed in other retinal
516 neurons, such as amicrine cells, which maintain separation by using their dendritic arbours
517 to repel neighbouring homotypic somata [40]; photoreceptors lack dendritic arbours, how-
518 ever.

519 My model selects non-doublable cones at the beginning of simulation runs, assuming
520 that the inability to form a double unit is an inherent property of certain cones. While blue
521 cones are never observed as double cone members in the Atlantic halibut or sablefish [22],
522 it is unclear whether non-blue centre cones are inherently incapable of forming double units
523 (or are disfavoured from doing so), or whether they are simply single cones left over from
524 the pairing process. A computational model that permits any non-blue cone to be paired
525 but leaves approximately 20% of cones unpaired may be able to elucidate which paradigm
526 of centre cone selection is more likely. This is a prospective direction for further research.

527 My model has several shortcomings whose resolution would strengthen its predictive
528 power. The simulated mosaics frequently have sizable “holes” in them—that is, regions
529 within the simulation that were populated with photoreceptors in the initial condition
530 but were empty in the final mosaic (Figure 3F). A likely cause of empty regions is that
531 the surrounding square units exhibit differing orientations and are unable to resolve these
532 differences to form a mosaic with a consistent orientation. Resolving the orientational dif-
533 ferences would require the dissolution of several square units and the reassembly of them
534 into a consistent orientation, which would necessitate escaping a local minimum in the
535 loss function. Getting “stuck” in a local minimum is a pervasive issue of gradient-based
536 optimization. However, the empty regions may be resolved by implementing a spring-like

537 restorative objective which compels cones to return to their original positions. Such an ob-
538 jective must not dominate the other objectives, providing just enough of an incentive for
539 the cones surrounding empty regions to fill them without entirely preventing cones from
540 leaving their initial positions.

541 While modelling cones as discs makes my model mathematically simple, it fails to cap-
542 ture the finer details of photoreceptor cells, whose influence on mosaic formation may be
543 significant. For example, adjacent cones exhibit cog-like cytoplasmic contacts, which, in tan-
544 dem with interlocking calyceal processes, have been hypothesized to mediate square mosaic
545 formation in Atlantic halibut [8]. In particular, a single cone may rotate in a cog-like fashion
546 with surrounding double cones to orient the double cones into a square unit arrangement
547 (see Figure 6 of [8]). A model which captures these details may provide greater insight into
548 the cellular mechanisms which underlie the objectives.

549 My model suggests that square mosaic formation is possible even under the assumption
550 that double cones are formed from randomly selected pairs of single cones. What remains to
551 be seen, however, is the effect that the scheme for forming double cones has on simulation
552 performance. It is conceivable that two single cones that are adjacent in the initial condition
553 would be more likely to pair than two cones at a distance of 2δ , yet both pairs have an
554 equal probability of forming a double cone in my model. More sophisticated schemes of
555 double cone formation, such as weighting the probability of double cone formation based
556 on proximity, are a prospective direction for further research.

557 Any biological mechanism which realizes the proposed objectives is unlikely to do so in a
558 manner that reflects L-BFGS-B optimization. This is less of an issue for loss functions with
559 simple energy landscapes, for which there is only one local minimum; alternative means of
560 optimization are likely to converge on the same minimum. However, the energy landscape for
561 f is quite rugged, with many local minima. Perturbing the positions of cones in the initial
562 condition by only 1/10 of a single cone diameter was sufficient to yield vastly different
563 terminal mosaics, although the performance of the unperturbed and perturbed simulations
564 appeared similar in informal testing. Trying different optimization schemes which better
565 handle rugged energy landscapes is a promising direction for future research, as it may
566 allow mosaics to escape local optima, resolving inconsistencies in square unit orientation
567 and improving regularity. Metropolis-Hastings approaches, which are less prone to getting
568 stuck in local minima, have been used to minimize loss functions in models of cell populations
569 [31, 32]; these algorithms are intractably slow for this problem, however, as f has hundreds or
570 even thousands of input dimensions. Basin-hopping, which combines stochastic optimization
571 techniques with gradient information [41], may be a suitable candidate for minimizing f .

572 This model has achieved modest success in modelling the transition from the hexagonal
573 mosaic to the square mosaic. A compelling direction for subsequent research would be to
574 apply this model to the assembly of mosaics at the retinal margin, where proliferating
575 cells expand an existing regular mosaic, such as the row mosaic in zebrafish and the square

576 mosaic in Atlantic halibut [17, 22]. Simulating peripheral mosaic assembly would require the
577 implementation of a mechanism for adding new cones. The initial condition would include
578 a partially assembled adult mosaic which proliferating cells affix to, expanding the mosaic
579 pattern.

580 **5 Conclusion**

581 This thesis provides the first computational model for the transformation of hexagonal
582 mosaics into square mosaics. The model uses real hexagonal mosaics from premetamorphic
583 Atlantic halibut and sablefish as initial conditions and numerically optimizes a loss function
584 to yield square mosaics. The simulated mosaics achieved single cone VARIs comparable
585 to those of retinal square mosaics in both species. The introduction of the square mosaic
586 score allowed for a more discriminate characterization of square mosaics and affirmed the
587 similarities between the simulated and retinal mosaics. Should these results be reproducible
588 for additional initial conditions, they suggest a developmental program for the transition
589 from hexagonal to square mosaic, which is estimated to occur in over 25% of all vertebrates,
590 including every marine fish observed thus far.

591 The model proposes two objectives that cones should fulfill to realize the transition
592 from hexagonal to square mosaic. The first objective is maximizing contacts between non-
593 doublable cones and the members of double cones. In the sablefish initial condition, non-
594 doublable cones are simply blue cones. In the Atlantic halibut, for which there are insuffi-
595 ciently many blue cones in the initial conditions to form a square mosaic using solely blue
596 centre cones, non-doublable cones also include a subset of the non-blue cones. The second
597 objective is preserving a minimum distance between non-doublable cones, suggesting that
598 the separation observed between blue cones in hexagonal mosaics is not intrinsically pre-
599 served but must be actively maintained as mosaic development progresses. The molecular
600 mechanisms which realize these objectives are yet to be determined, suggesting an exciting
601 new direction for continued research in retinal biology.

602 Bibliography

- 603 [1] D.H. Brainard. Color and the cone mosaic. *Annu. Rev. Vis. Sci.*, 1:519–546, 2015.
- 604 [2] T. Ebrey and Y. Koutalos. Vertebrate photoreceptors. *Prog. Retin. Eye Res.*, 20:49–91,
605 2001.
- 606 [3] F.I. Hárosi. An analysis of two spectral properties of vertebrate visual pigments. *Vis.
607 Res.*, 34:1359–1367, 1994.
- 608 [4] S. Yokoyama. Evolution of dim-light and color vision pigments. *Annu. Rev. Genom.
609 Hum. Genet.*, 9:259–282, 2008.
- 610 [5] P. Bartel, Y. Yoshimatsu, F.K. Janiak, and T. Baden. Spectral inference reveals prin-
611 cipal cone-integration rules of the zebrafish inner retina. *Curr. Biol.*, 31:5214–5226,
612 2021.
- 613 [6] S. Frau, I. Novales Flamarique, P.W. Keeley, B.E. Reese, and J.A. Muñoz-Cueto. Stray-
614 ing from the flatfish retinal plan: Cone photoreceptor patterning in the common sole
615 (*Solea solea*) and the Senegalese sole (*Solea senegalensis*). *J. Comp. Neurol.*, 528:2283–
616 2307, 2020.
- 617 [7] F.I. Hárosi and I. Novales Flamarique. Functional significance of the taper of vertebrate
618 cone photoreceptors. *J. Gen. Physiol.*, 139:159–187, 2012.
- 619 [8] I. Novales Flamarique and L.A. Grebinsky. Single cones give rise to multi-cone types
620 in the retinas of fishes. *Sci. Rep.*, 15:7823, 2025.
- 621 [9] B. Sajdak, Y. Sulai, C.S. Langlo, G. Luna, S.K. Fisher, D.K. Merriman, and A. Dubra.
622 Noninvasive imaging of the thirteen-lined ground squirrel photoreceptor mosaic. *Vis.
623 Neurosci.*, 33:e003, 2016.
- 624 [10] C.A. Curcio, K.R. Sloan, R.E. Kalina, and A.E. Hendrickson. Human photoreceptor
625 topography. *J. Comp. Neurol.*, 292:497–523, 1990.
- 626 [11] L. Sawides, A. de Castro, and S.A. Burns. The organization of the cone photoreceptor
627 mosaic measured in the living human retina. *Vis. Res.*, 132:34–44, 2017.
- 628 [12] K.L. Hoke, B.I. Evans, and R.D. Fernald. Remodeling of the cone photoreceptor mosaic
629 during metamorphosis of flounder (*Pseudopleuronectes americanus*). *Brain Behav.
630 Evol.*, 68:241–254, 2006.
- 631 [13] J. Shand, M.A. Archer, and N.T. Cleary. Retinal development of West Australian
632 dhufish, *Glaucosoma hebraicum*. *Vis. Neurosci.*, 18:711–724, 2001.

- 633 [14] J. Shand, M.A. Archer, and S.P. Collin. Ontogenetic changes in the cone photoreceptor
634 mosaic in a fish, the black bream, *Acanthopagrus butcheri*. *J. Comp. Neurol.*, 412:203–
635 217, 1999.
- 636 [15] Y.A. Kram, S. Mantey, and J.C. Corbo. Avian cone photoreceptors tile the retina as
637 five independent, self-organizing mosaics. *PLOS One*, 5:e8992, 2010.
- 638 [16] E.R. Loew, V.I. Govardovskii, P. Röhlich, and A. Szél. Microspectrophotometric and
639 immunocytochemical identification of ultraviolet photoreceptors in geckos. *Vis. Neurosci.*, 13:247–256, 1996.
- 641 [17] W.T. Allison, L.K. Barthel, K.M. Skebo, M. Takechi, S. Kawamura, and P.A. Raymond.
642 Ontogeny of cone photoreceptor mosaics in zebrafish. *J. Comp. Neurol.*, 518:4182–4195,
643 2010.
- 644 [18] A.S. French, A.W. Snyder, and D.G. Stavenga. Image degradation by an irregular
645 retinal mosaic. *Biol. Cybern.*, 27:229–233, 1977.
- 646 [19] P.W. Keeley, S.J. Eglen, and B.E. Reese. From random to regular: Variation in the
647 patterning of retinal mosaics. *J. Comp. Neurol.*, 528:2135–2160, 2020.
- 648 [20] B.E. Reese and P.W. Keeley. Design principles and developmental mechanisms under-
649 lying retinal mosaics. *Biol. Rev.*, 90:854–876, 2015.
- 650 [21] J.S. Nelson, T.C. Grande, and M.V.H. Wilson. *Fishes of the world*. John Wiley &
651 Sons, Inc., Hoboken, NJ, 2016.
- 652 [22] K. Bolstad and I. Novales Flamarique. Photoreceptor distributions, visual pigments
653 and the opsin repertoire of Atlantic halibut (*Hippoglossus hippoglossus*). *Sci. Rep.*,
654 12:8062, 2022.
- 655 [23] K. Bolstad and I. Novales Flamarique. Chromatic organization of cone photorecep-
656 tors during eye migration of Atlantic halibut (*Hippoglossus hippoglossus*). *J. Comp.*
657 *Neurol.*, 531:256–280, 2023.
- 658 [24] I. Savelli, I. Novales Flamarique, T. Iwanicki, and J.S. Taylor. Parallel opsin switches
659 in multiple cone types in the starry flounder retina: Tuning visual pigment composition
660 for a demersal life style. *Sci. Rep.*, 8:4763, 2018.
- 661 [25] M.M. Mader and D.A. Cameron. Photoreceptor differentiation during retinal develop-
662 ment, growth, and regeneration in a metamorphic vertebrate. *J. Neurosci.*, 24:11463–
663 11472, 2004.
- 664 [26] H. Nunley, M. Nagashima, K. Martin, A. Lorenzo Gonzalez, S.C. Suzuki, D.A. Norton,
665 R.O.L. Wong, P.A. Raymond, and D.K. Lubensky. Defect patterns on the curved
666 surface of fish retinae suggest a mechanism of cone mosaic formation. *PLOS Comput.*
667 *Biol.*, 16:e1008437, 2020.
- 668 [27] G. Salbreux, L.K. Barthel, P.A. Raymond, and D.K. Lubensky. Coupling mechanical
669 deformations and planar cell polarity to create regular patterns in the zebrafish retina.
670 *PLOS Comput. Biol.*, 8:e1002618, 2012.

- 671 [28] S. Tohya, A. Mochizuki, and Y. Iwasa. Difference in the retinal cone mosaic pattern
672 between zebrafish and medaka: cell-rearrangement model. *J. Theor. Biol.*, 221:289–300,
673 2003.
- 674 [29] S. Tohya, A. Mochizuki, and Y. Iwasa. A mathematical model explaining species
675 diversity of cone mosaic in fish retina. *Dev. Growth Differ.*, 43:S68, 2001.
- 676 [30] Y. Nishiwaki, T. Oishi, F. Tokunaga, and T. Morita. Three-dimensional reconstitution
677 of cone arrangement on the spherical surface of the retina in the medaka eyes. *Zool.
678 Sci.*, 14:795–801, 2009.
- 679 [31] J.M. Osborne, A.G. Fletcher, J.M. Pitt-Francis, P.K. Maini, and D.J. Gavaghan. Comparing
680 individual-based approaches to modelling the self-organization of multicellular
681 tissues. *PLOS Comput. Biol.*, 13:1–34, 2017.
- 682 [32] P. Pathmanathan, J. Cooper, A. Fletcher, G. Mirams, P. Murray, J. Osborne, J. Pitt-
683 Francis, A. Walter, and S.J. Chapman. A computational study of discrete mechanical
684 tissue models. *Phys. Biol.*, 6:036001, 2009.
- 685 [33] D. Drasdo and S. Hoehme. A single-cell-based model of tumor growth in vitro: Mono-
686 layers and spheroids. *Phys. Biol.*, 2:133–147, 2005.
- 687 [34] D. Drasdo and M. Loeffler. Individual-based models to growth and folding in one-
688 layered tissues: intestinal crypts and early development. *Nonlinear Anal., Theory
689 Methods Appl.*, 47:245–256, 2001.
- 690 [35] A. Davison, K. Gierke, J. Brandstätter, and N. Babai. Functional and structural
691 development of mouse cone photoreceptor ribbon synapses. *Invest. Ophthalmol. Vis.
692 Sci.*, 63:21, 2022.
- 693 [36] M. Blondel, Q. Berthet, M. Cuturi, R. Frostig, S. Hoyer, F. Llinares-López, F. Pe-
694 dregosa, and J. Vert. Efficient and modular implicit differentiation. In *Proceedings of
695 the 36th International Conference on Neural Information Processing Systems*, NIPS
696 ’22, Red Hook, NY, 2022. Curran Associates Inc.
- 697 [37] C. Kostic and Y. Arsenijevic. Animal modeling for inherited central vision loss. *J.
698 Pathol.*, 238:300–310, 2015.
- 699 [38] A. Mochizuki. Pattern formation of the cone mosaic in the zebrafish retina: A cell
700 rearrangement model. *J. Theor. Biol.*, 215:345–361, 2002.
- 701 [39] J. Zou, X. Wang, and X. Wei. Crb apical polarity proteins maintain zebrafish reti-
702 nal cone mosaics via intercellular binding of their extracellular domains. *Dev. Cell*,
703 22:1261–1274, 2012.
- 704 [40] C. Kozlowski, S.E. Hadyniak, and J.N. Kay. Retinal neurons establish mosaic pat-
705 ttering by excluding homotypic somata from their dendritic territories. *Cell Rep.*,
706 43:114615, 2024.
- 707 [41] D.J. Wales and J.P.K. Doye. Global optimization by basin-hopping and the lowest
708 energy structures of Lennard-Jones clusters containing up to 110 atoms. *J. Phys.
709 Chem. A*, 101:5111–5116, 1997.